Electronic Supplementary Material

All-Vanadium Dual Circuit Redox Flow Battery for Renewable Hydrogen Generation and Desulfurisation

Pekka Peljo,[a] Heron Vrubel,[a], Véronique Amstutz,[a] Justine Pandard,[a] Joana Morgado,[a,e] Annukka Santasalo-Aarnio,[c] David Lloyd,[b] Frédéric Gumy,[a] C. R. Dennison,[a] Kathryn E. Toghill,[d] Hubert H. Girault,[a,]*

[a] Laboratoire d'Electrochimie Physique et Analytique (LEPA)
École Polytechnique Fédérale de Lausanne (EPFL) - Valais Wallis
Rue de l'Industrie 17
Case Postale 440
CH-1951 Sion

[b] Department of Materials Science and Engineering,
Aalto University
Vuorimiehentie 2,
PO Box 16200,
00076 Aalto,
Finland

[c] Department of Chemistry
Aalto University
Kemistintie 1,
PO Box 16100,
0076 Aalto,
Finland

[d] Department of Chemistry
Lancaster University
Lancaster,
LA1 4YB,
United Kingdom

[e] Present address: Department of Energy and Process Engineering,
Norwegian University of Science and Technology,
7491 Trondheim,
Norway

ESI-1. Sythesis and characterization of Mo_2C supported on alumina

Mo_2C/Al_2O_3 was synthesized according to the procedure of Lin *et al.*[S1] shown in Scheme S1. Briefly, it is based on the impregnation of alumina beads with an ammonium heptamolybdate precursor solution at 40°C. 5 wt % and 10% wt% Mo2C were prepared, by adjusting the concentration of the precursor to the volume of solution absorbed by the alumina support during the impregnation step. In order to obtain molybdenum oxides (MoO_x), this step was followed by a 4 h heat treatment under a 1 L/min nitrogen flow (N_2 purity 99.999%, Carbagas), at 400°C in a tubular furnace (OTF-1200X, MTI Corporation, 2.5 kW). MoO_x was then reduced to metallic molybdenum by exposing it to hydrogen (purity 99.999%, Carbagas) at 850°C for 2 h, and further carburized by a 20% : 80% methane-hydrogen gas mixture (CH_4 technical grade, Carbagas) at 675°C for 2 h in order to obtain the final molybdenum carbide catalyst. The initially white alumina beads appeared totally black after the deposition of catalyst. Moreover, in order to remove the catalyst particles which were only weakly attached to the support, the synthesized catalyst beads were washed thoroughly with deionized water and dried under vacuum. The synthesized catalysts were characterized by high-resolution scanning electron microscopy (HRSEM, Zeiss Merlin, column Gemini II), and Brunauer-Emmett-Teller (BET) measurements of the surface area were conducted for the as-received alumina and both prepared catalysts using a Chemisorption Analyzer (Micromeritics Autochem II) with a gaseous mixture of He containing 30% N_2.

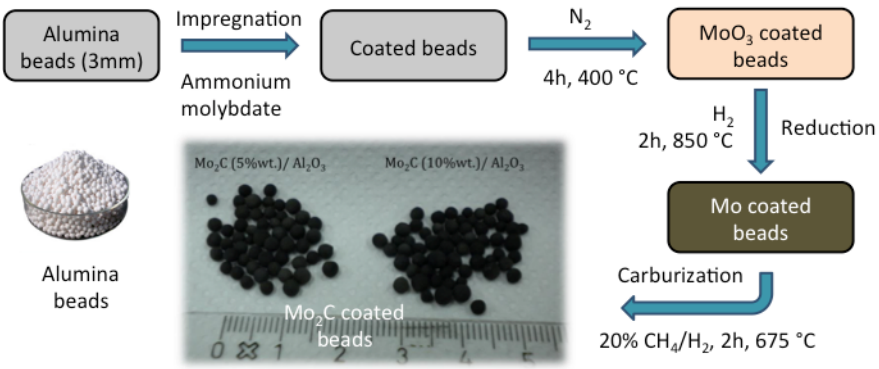

Scheme S1. Synthesis procedure of Mo_2C coated alumina beads.

SEM images showed the presence of nanoparticles of Mo_2C formed at the surface of the alumina support (Figure 6). The as-received alumina support exhibits a compressed pelleted "flake" structure with numerous micropores and mesopores. Smaller pores are not clearly visible in Figure 6, but were observed during the examination with the microscope. It can be clearly seen that Mo_2C nanoparticles were deposited on the support during the synthesis. They have a size of approximately 20-30 nm for 5 wt% Mo_2C/Al_2O_3 and 40-60 nm for 10 wt% Mo_2C/Al_2O_3. Moreover, denser regions were observed on the latter samples, where the nanoparticles are sintered together, almost leading to a full layer of catalyst at the surface of the support. This implies a decrease of the active surface area of the catalyst.

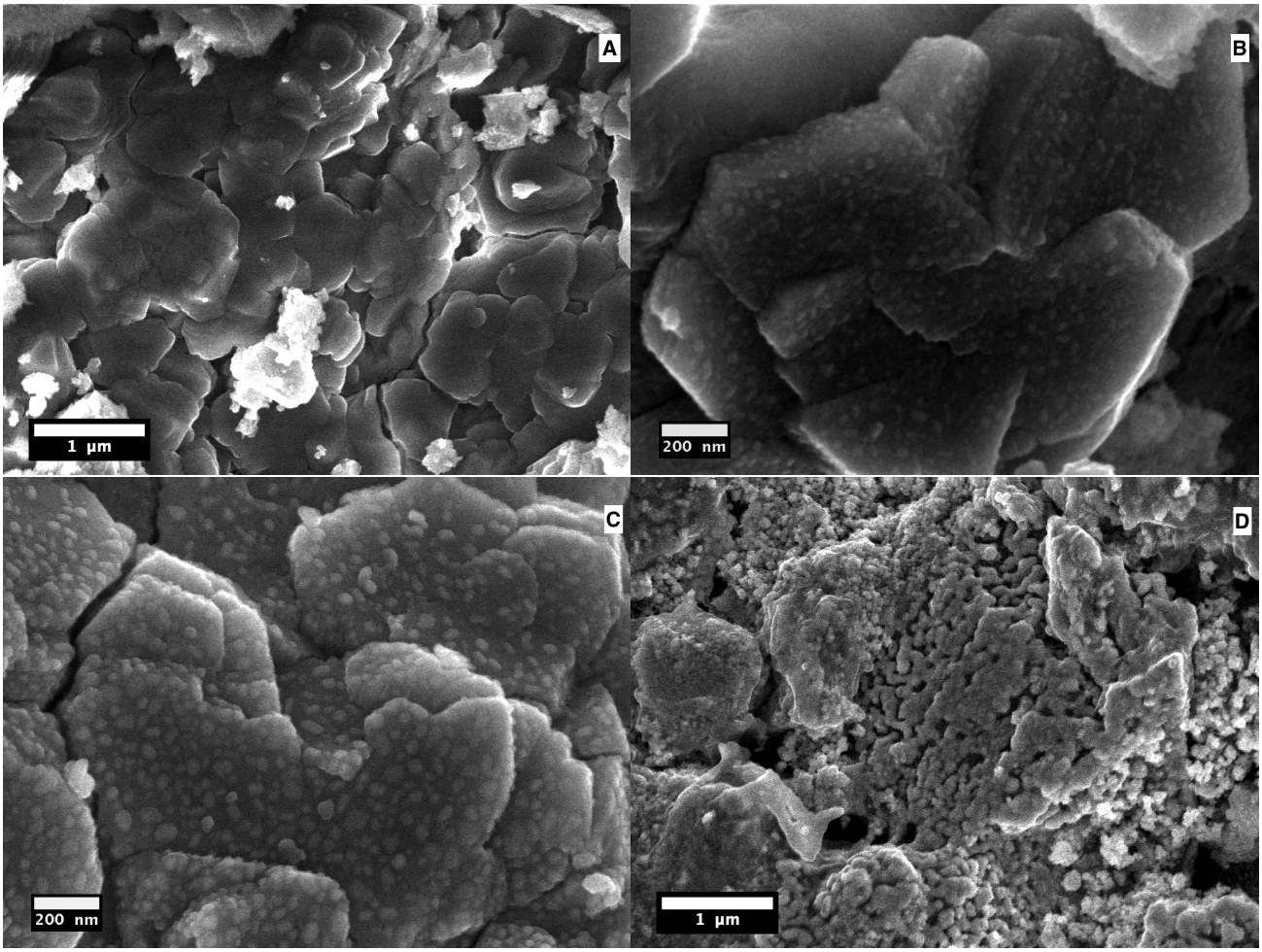

Figure S1. HRSEM pictures of as-received alumina (A), 5% Mo_2C/Al_2O_3 (B) and 10% Mo_2C/Al_2O_3 (C and D represent two different spots).

Brunauer-Emmett-Teller measurements of the surface area showed that the original alumina support has a very high BET area of 320 m^2 g^{-1}, which decreases due to the deposition of the catalyst particles to 126 and 118 m^2 g^{-1} for 5 % and 10 % Mo_2C/Al_2O_3. This could indicate either a change of the alumina structure during the catalyst synthesis or the blockage of alumina (nano)pores by the catalyst particles. The higher value of specific area for the lower loading may be related to less pores blocked and to a higher dispersion of the particles, as corroborated by the SEM pictures.

The stability of the 5 wt% Mo_2C/Al_2O_3 catalyst (0.4 g) was tested in absence of stirring, in a 0.35 M V(II) and 1.65 M H_2SO_4 solution (4 mL) by first fully reacting V(II) on the catalyst and then collecting the catalyst (in the glovebox) at the end of the reaction and reusing it for the next cycle. In total five cycles were evaluated by monitoring the increase of pressure due to the production of hydrogen. This experiment showed that the rate of reaction decreased between the first and the second cycles, but did not decrease significantly during the 4 last cycles, indicating a relatively good stability of the catalyst in these conditions. However, when the catalyst was tested with higher V(II) concentrations (up to 1 M V(II)), small particles of catalysts floating in the solution were observed. This could be explained by the formation of hydrogen bubbles in the pores of the alumina support, inducing the detachment of the small aggregated alumina particles from the bead.

This mechanism of catalyst breakdown was further verified by testing the mechanical stability of the catalyst by subjecting the 5 wt% Mo_2C/Al_2O_3 beads to stirring in 1 M sulfuric acid for 45 min both at 450 and 900 rotations per minute (rpm). As shown on Figure 7, the solution became darker at 450 rpm, and almost black at 950 rpm due to the disintegration of the alumina particles. Indeed, filtering this solution with a paper filter and analysis of the filtrated solution showed that only a small quantity of nanoparticles were detached from the support, indicating a strong interaction between the support and the catalyst. However the alumina support was broken in small particles as the “flakes” forming the alumina beads, visible in Figure 6, were apparently only weakly interconnected and can detach under mechanical stress. This simple experiment also facilitated the observation that the interior of the beads was also covered with nanoparticles, as they kept a strong black color. This suggests on one side that the impregnation synthesis method was appropriate for such

a high-surface area support and on the other side that hydrogen could also be formed in the pores of the alumina beads.

As a consequence of these experiments and in particular due to the lack of mechanical stability of the alumina support, it was decided to find another catalyst support.

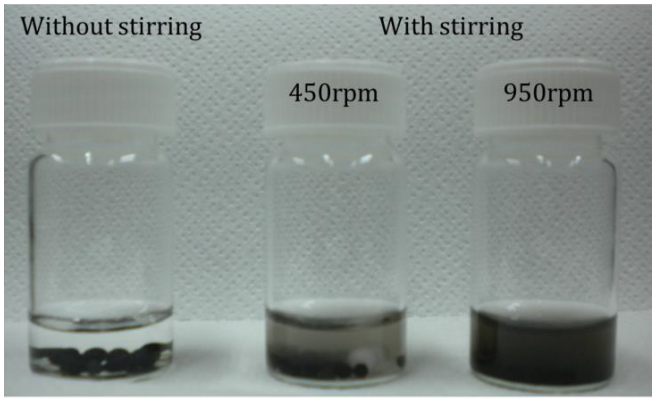

Figure S2. Mechanical stability of the 5 wt% Mo_2C/Al_2O_3 stirred with a magnetic stirrer at different rates.

ESI-2. Measurements of the rate of hydrogen evolution for Mo_2C supported on Denstone

1 mL of 1.6 M V(II) solution was injected in a reactor closed by a silicon septum using a syringe. A second syringe needle was used for keeping an atmospheric pressure initially. Previously to the injection, 10 beads of catalyst (weighted) and a magnetic stirrer were added in the reactor and the reactor was purge with nitrogen for 2 minutes. The reactor atmosphere was then connected to a differential pressure sensor (40PC100G2A, Honeywell, 0-100 psi). The signal of this sensor was calibrated by the consecutive additions of 0.5 air with a syringe in the reactor, starting from atmospheric pressure. Moreover, the air tightness of the reactor was also tested for 20 minutes close to the saturation limit. During the catalytic reaction, the stirring rate was 200 rpm (except for Sample 1), the temperature was maintained constant at 27 °C in a mixed oil bath. The atmospheric pressure was considered constant for the present set of measurements (1.1015 bar). The rate of hydrogen evolution normalized by the catalyst mass (including the mass of the support) as a function of time is shown in

Figure S3. The results show that Mo_2C supported on ceramic beads is an active catalyst for hydrogen evolution.

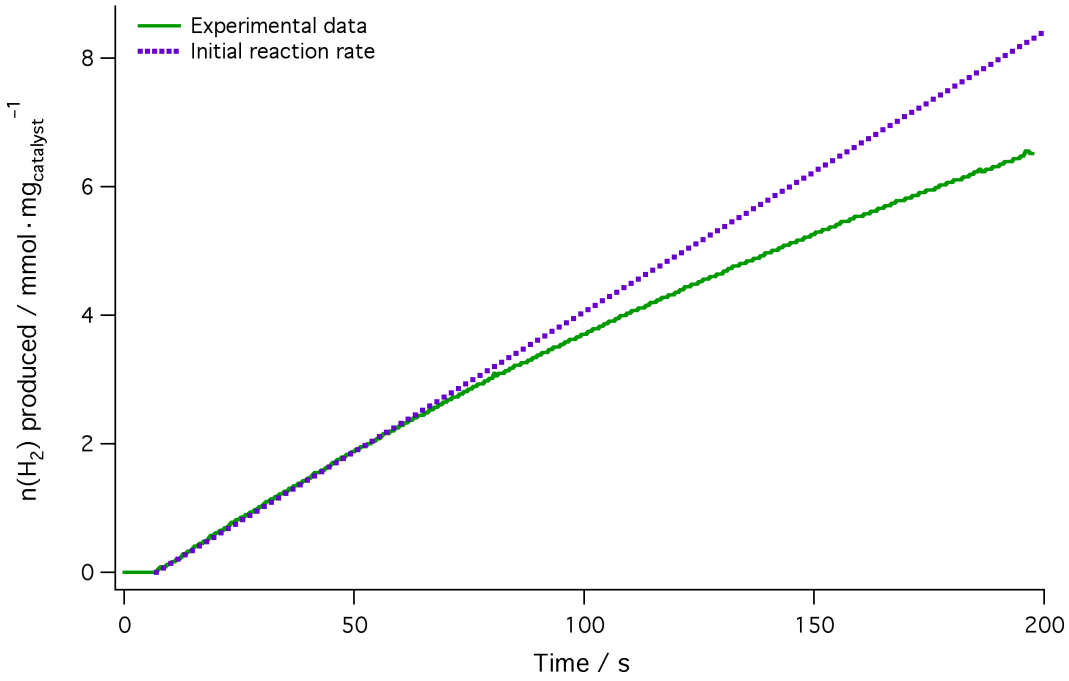

Figure S3. The rate of hydrogen evolution normalized by the catalyst mass (including the mass of the support) as a function of time

ESI-3. Thermodynamics and Efficiency Calculations

To evaluate the efficiencies of the different options, most common way is to compare the heat available from combustion of the produced fuel to the energy required to produce it. Typically, higher heating value (HHV) and lower heating value (LHV) are used to for these calculations, where reactants at 25 °C are combusted to products at 25 °C (HHV) or 150 °C (LHV). The combustion reactions for hydrogen and the different reactants used in the chemical discharge of the positive electrolyte of the RFB are (for HHV with both reactants and products at 25 °C):

$$H_2\,(g) + \tfrac{1}{2}\,O_2\,(g) \rightarrow H_2O\,(l) \qquad (S1)$$

N_2H_4 (l) + O_2 (g) → N_2 (g) + 2 H_2O (l) (S2)

SO_2 (g) + ½ O_2 (g) + H_2O (l) → H_2SO_4 (l) (S3)

H_2S (g) + ½ O_2 (g) → S (s) + H_2O (l) (S4)

The reaction enthalpies can be calculated from the difference of the standard formation enthalpies of products and reactants,[S2] and this calculation directly gives the HHV. For calculations of LHV, we can consider that each reaction produces products at the state where they are at 150 °C (e.g. H_2O will be gas, other products will stay is the states described in equations above), and all the products need to be heated up from 25 to 150 °C. This can be done when heat capacities at constant pressure are known, and by assuming that they do not significantly change with the temperature. The results are summarized in Table S1.

Table S1. Higher and lower heating values of various fuels, calculated based on thermodynamic data.[S1]

Reaction	HHV, kJ mol^{-1}	LHV, kJ mol^{-1}
$H_2 + 1/2O_2 \rightarrow H_2O$	286	238
$N_2H_4 + O_2 \rightarrow N_2 + 2\ H_2O$	622	522
$SO_2 + 1/2\ O_2 + H_2O \rightarrow H_2SO_4$	231	214
$H_2S + 1/2\ O_2 \rightarrow S + H_2O$	265	214

On the other hand, if hydrogen is utilized in a fuel cell to produce electricity, it makes more sense to use the Gibbs energy change for reaction S1, (as a fuel cell can theoretically utilize the total Gibbs energy change of the reaction) corresponding to −237 kJ mol^{-1} (or −228 kJ mol^{-1} if the product is water vapour) of chemical energy converted into electricity. [S1]

If we consider the reactor producing hydrogen at 10 mol h^{-1}, this corresponds to

production of fuel with the energy content of 2.86 or 2.38 MJ h^{-1} (HHV and LHV). As charging the battery optimally consumes 135 J of DC electricity (140 J of AC electricity due to conversion losses) per mole of vanadium (on each side), and two molecules of V^{2+} is required to produce one mole of hydrogen, the energy consumption of the battery to produce the required amount of charged electrolyte is 2.65 MJ (or 2.74 MJ considering AC-DC conversion losses). Hence, in one hour the process produces hydrogen for 2.8 MJ while consuming 2.65 MJ of renewable electricity. But of course, the total efficiency of the system depends also on the other side: as the energy input in the form of the reactants needs to be taken into account:

- **Hydrazine**. Production of ten moles of hydrogen by dual circuit redox flow battery requires consumption of five moles of hydrazine to discharge by an equal amount the positive electrolyte. The heat available from combustion of hydrazine would be 3.11 MJ (HHV) or 2.66 MJ (LHV).
- **Sulfur Dioxide**. As production of ten moles of hydrogen by dual circuit redox flow battery requires the consumption of an equal amount of SO_2 to discharge equally the positive electrolyte, the heat available from combustion of SO_2 would be 2.31 MJ (HHV) or 2.14 MJ (LHV).
- **Hydrogen Sulfide**. As previously, ten moles of hydrogen requires also an equal amount of H_2S, corresponding to the heat of 2.65 MJ (HHV) or 2.14 MJ (LHV) available from combustion.

The efficiency for each considered case was calculated with the following equation:

$$\eta = \frac{\text{Energy in hydrogen + Electricity out}}{\text{Electricity in + Energy in reactant}} \qquad \text{(S5)}$$

where both energy in hydrogen and the energy in reactant is given in either LHV or HHV, used electricity is either DC or AC, and electricity is produced only in a case where SO_2/V(V) fuel cell is employed. Consuming 10 mol h^{-1} of SO_2 requires a current of 536 A, and if this current is drawn at the optimum voltage of the fuel cell at 0.3 V, it produces 160 Wh of electricity in one hour, or 579 kJ h^{-1}. Now these numbers can be utilized to evaluate the efficiencies of different cases with equation S5, summarized in Table S2.

Table S2. The efficiency of the dual circuit redox flow battery system considering either AC or DC electricity used to charge the battery, considering either chemical discharge of the positive electrolyte with N_2H_4, SO_2 or H_2S, or electrochemical discharge with SO_2/V(V) fuel cell (FC), for both HHV and LHV.

	HHV				LHV			
	N_2H_4	SO_2	H_2S	SO_2, FC	N_2H_4	SO_2	H_2S	SO_2, FC
DC electricity	49.2%	57.0%	53.4%	68.5%	45.5%	50.0%	49.9%	61.9%
AC electricity	48.4%	56.0%	52.5%	67.3%	44.7%	49.0%	49.0%	60.8%

Of course, if we consider that hydrogen will be converted into electricity with a fuel cell, the maximum system efficiency is decreased to 83% of the present calculations, as this is the maximum thermodynamic efficiency of a fuel cell (95% for LHV).

ESI-4. Supplementary Videos

The following supporting videos are included in the supporting information:

- **Supplementary Video S1:** Indirect Hydrogen Evolution by V^{2+} solution catalyzed by Mo_2C catalyst supported on beads
- **Supplementary Video S2:** Secondary Circuit for Hydrogen Evolution
- **Supplementary Video S3:** Discharge of the Positive Vanadium Electrolyte by Hydrazine

- **Supplementary Video S4:** Discharge of the Positive Vanadium Electrolyte by Sulfur Dioxide
- **Supplementary Video S5:** Discharge of the positive vanadium electrolyte by Hydrogen Sulfide.

ESI-5. Supplementary References

S1 S. S. Y. Lin, W. J. Thomson, T. J. Hagensen and S. Y. Ha, *Applied Catalysis A: General*, 2007, **318**, 121-127.

S2 in *CRC Handbook of Chemistry and Physics*, eds. W. M. Haynes, T. J. Bruno and D. R. Lide, Taylor and Francis Group, LLC, 96th edn., 2016, pp. 5:4-42.